

## Ferroelectric Properties of RbNbO<sub>3</sub> and RbTaO<sub>3</sub>

A. I. Lebedev

Moscow State University, Moscow, 119991 Russia

e-mail: swan@scon155.phys.msu.ru

Received July 30, 2014

**Abstract**—Phonon spectra of cubic rubidium niobate and rubidium tantalate with the perovskite structure are calculated from first principles within the density functional theory. Based on the analysis of unstable modes in phonon spectra, symmetries of possible distorted phases are determined, their energies are calculated, and it is shown that  $R3m$  is the ground-state structure of RbNbO<sub>3</sub>. In RbTaO<sub>3</sub>, the ferroelectric instability is suppressed by zero-point lattice vibrations. For ferroelectric phases of RbNbO<sub>3</sub>, spontaneous polarization, piezoelectric, nonlinear optical, electro-optical, and other properties as well as the energy band gap in the LDA and  $GW$  approximations are calculated. The properties of rhombohedral RbNbO<sub>3</sub> are compared with those of rhombohedral KNbO<sub>3</sub>, LiNbO<sub>3</sub>, and BaTiO<sub>3</sub>.

DOI: 10.1134/S1063783415020237

The possibility of ferroelectricity in rubidium niobate and rubidium tantalate with the perovskite structure was discussed by Smolenskii and Kozhevnikova [1] and then by Megaw [2] in the early 1950s. In [1], the authors referred to unpublished data by V.G. Prokhvatilov who detected the tetragonal RbTaO<sub>3</sub> phase with  $a = 3.92 \text{ \AA}$ ,  $c = 4.51 \text{ \AA}$  exhibiting a phase transition near 520 K; in [2], these data were simply cited. However, further studies have shown that, unlike lithium, sodium, and potassium niobates, RbNbO<sub>3</sub> and RbTaO<sub>3</sub> crystallize in individual crystal structures with triclinic  $P\bar{1}$  symmetry for RbNbO<sub>3</sub> and monoclinic  $C2/m$  one for RbTaO<sub>3</sub> [3–5] when prepared at atmospheric pressure. To obtain these materials with the perovskite structure, they should be prepared at high pressures (65–90 kbar) [6]. Due to the difficulties in synthesis of RbNbO<sub>3</sub> and RbTaO<sub>3</sub> with the perovskite structure, the properties of these crystals have been studied very little.

The phase diagrams of Rb<sub>2</sub>O–Nb<sub>2</sub>O<sub>5</sub> and Rb<sub>2</sub>O–Ta<sub>2</sub>O<sub>5</sub> systems were studied in [7, 8]. RbNbO<sub>3</sub> is formed by the peritectic reaction and decomposes above 964°C [7]. RbTaO<sub>3</sub> decomposes above 600°C probably due to the peritectic reaction too [8]. Rubidium-containing ferroelectric materials in the BaNb<sub>2</sub>O<sub>6</sub>–NaNbO<sub>3</sub>–RbNbO<sub>3</sub> system with the tungsten-bronze structure have high electro-optical properties that substantially exceed those of lithium niobate [9, 10]. In [11], the possibility of using rubidium niobate and rubidium tantalate for photoelectrochemical decomposition of water was discussed. In [12], it was proposed to use the delamination of RbTaO<sub>3</sub> structure to produce porous TaO<sub>3</sub> nanomembranes

with pore sizes of  $1.3 \times 0.6$  and  $1.1 \times 1.1 \text{ \AA}$ , which can be used for selective filtration of lithium ions.

The lack of knowledge on the properties of compounds under consideration appears, in particular, in contradictory data on the ferroelectric properties of RbTaO<sub>3</sub>. For example, the existence of the phase transition at 520 K in the tetragonal phase was reported in [1], whereas the data of [6] showed that RbTaO<sub>3</sub> prepared at high pressure has the cubic perovskite (or close to it) structure. At 300 K, the structure of RbNbO<sub>3</sub> is similar to that of the orthorhombic BaTiO<sub>3</sub>, and the data of differential thermal analysis indicate phase transitions in it at 15, 155, and 300°C [6].

In this work, the equilibrium structures of RbNbO<sub>3</sub> and RbTaO<sub>3</sub> were determined from first-principles calculations, and spontaneous polarization, dielectric constant, piezoelectric and elastic moduli, nonlinear optical and electro-optical properties as well as the energy band gaps in the LDA and  $GW$  approximations were calculated for these crystals.

The first-principles calculations were performed within the density functional theory using the ABINIT software [13]. The exchange–correlation interaction was described in the local density approximation (LDA). The optimized norm-conserving pseudopotentials for Nb, Ta, and O atoms used in these calculations were taken from [14]. The non-relativistic pseudopotential for the Rb atom (electronic configuration  $4s^2 4p^6 5s^0$ ) was constructed according to the scheme of [15] using the OPIUM program [16] with the following parameters:  $r_s = 1.68$ ,  $r_p = 1.72$ ,  $r_d = 1.68$ ,  $q_s = 7.07$ ,  $q_p = 7.27$ ,  $q_d = 7.07$ ,  $r_{\min} = 0.01$ ,  $r_{\max} = 1.52$ , and  $V_{\text{loc}} = 1.58 \text{ a.u.}$  (for notations, see [17]). The testing of the Rb pseudopotential on the  $P\bar{1}$  phase of

**Table 1.** Calculated lattice parameters and atomic coordinates in RbNbO<sub>3</sub> structures

Atom	Position	$x$	$y$	$z$
Phase $P\bar{1}$ $a = 5.0816 \text{ \AA}$ , $b = 8.3047 \text{ \AA}$ , $c = 8.7916 \text{ \AA}$ , $\alpha = 114.0625^\circ$ , $\beta = 93.3891^\circ$ , $\gamma = 95.1160^\circ$				
Rb2	1a	+0.00000	+0.00000	+0.00000
Rb1	1b	+0.00000	+0.00000	+0.50000
Rb3	2i	+0.41251	+0.70257	+0.09488
Nb1	2i	+0.49674	+0.28138	+0.35602
Nb2	2i	+0.02746	+0.51037	+0.30988
O1	2i	+0.10125	+0.39078	+0.82160
O2	2i	+0.23664	+0.42747	+0.50994
O3	2i	+0.28650	+0.71922	+0.45293
O4	2i	+0.29777	+0.37205	+0.19910
O5	2i	+0.33951	+0.05579	+0.27137
O6	2i	+0.78420	+0.27571	+0.22313
Phase $Pm\bar{3}m$ $a = 4.0291 \text{ \AA}$				
Rb	1a	+0.00000	+0.00000	+0.00000
Nb	1b	+0.50000	+0.50000	+0.50000
O	3c	+0.00000	+0.50000	+0.50000
Phase $P4mm$ $a = 4.0037 \text{ \AA}$ , $c = 4.1592 \text{ \AA}$				
Rb	1a	+0.00000	+0.00000	-0.00336
Nb	1b	+0.50000	+0.50000	+0.51818
O1	2c	+0.50000	+0.00000	+0.47446
O2	1b	+0.50000	+0.50000	-0.03654
Phase $Amm2$ $a = 3.9928 \text{ \AA}$ , $b = 5.7742 \text{ \AA}$ , $c = 5.7960 \text{ \AA}$				
Rb	2a	+0.00000	+0.00000	-0.00341
Nb	2b	+0.50000	+0.00000	+0.51447
O1	4e	+0.50000	+0.25496	+0.22842
O2	2a	+0.00000	+0.00000	+0.47735
Phase $R3m$ $a = 4.0571 \text{ \AA}$ , $\alpha = 89.8945^\circ$				
Rb	1a	-0.00308	-0.00308	-0.00308
Nb	1a	+0.51193	+0.51193	+0.51193
O	3b	-0.02115	+0.48415	+0.48415

RbNbO<sub>3</sub> and the  $C2/m$  phase of RbTaO<sub>3</sub>, which are stable at atmospheric pressure, showed its sufficiently high quality: the calculated lattice parameters and atomic coordinates in these phases (see Tables 1 and 2)

are in good agreement with the experimental data [3, 5]; small underestimates of the calculated lattice parameters are characteristic of the LDA approximation used in this work.

The lattice parameters and equilibrium atomic positions in the unit cells were determined from the condition when the residual forces acting on the atoms were below  $5 \times 10^{-6}$  Ha/Bohr (0.25 meV/Å) in the self-consistent calculation of the total energy with an accuracy better than  $10^{-10}$  Ha. The maximum energy of plane waves was 30 Ha for RbNbO<sub>3</sub> and 40 Ha for RbTaO<sub>3</sub>. Integration over the Brillouin zone was performed using a  $8 \times 8 \times 8$  Monkhorst–Pack mesh. The spontaneous polarization in ferroelectric phases was calculated by the Berry phase method. The phonon spectra, dielectric constants, piezoelectric and elastic moduli were calculated within the density-functional perturbation theory similarly to [17]. Nonlinear optical and electro-optical properties were calculated using the technique described in [18]. All physical properties presented in this work were calculated for the theoretical lattice parameter.

The phonon spectrum of RbNbO<sub>3</sub> in the cubic  $Pm\bar{3}m$  phase is shown in Fig. 1. This spectrum contains a band of unstable modes characteristic of ferroelectric chain instability which was first observed in KNbO<sub>3</sub> [19]. At the center of the Brillouin zone, this mode has the  $\Gamma_{15}$  symmetry, is triply degenerate, and describes the ferroelectric distortion of structure. The structures appearing upon condensation of the  $X_5$  and  $M'_3$  modes are characterized by antiparallel orientation of polarization in neighboring ...–O–Nb–O–... chains.

The energies of all RbNbO<sub>3</sub> phases formed upon condensation of the above unstable modes are given in Table 3. Among these phases, the  $R3m$  phase has the lowest energy. The phonon spectrum calculations for the  $R3m$  phase show that the frequencies of all optical phonons at the center of the Brillouin zone and at high-symmetry points at its boundary are positive; the determinant and all leading principal minors constructed of elastic moduli tensor components are also positive. This means that the  $R3m$  phase is the ground-state structure of RbNbO<sub>3</sub>. The calculated lattice parameters and atomic coordinates in this phase are given in Table 1. As the same sequence of phases as in BaTiO<sub>3</sub> is supposed in rubidium niobate with the perovskite structure [6], the lattice parameters and atomic coordinates in two other ferroelectric phases are also given in this table. The lattice parameters calculated for the orthorhombic RbNbO<sub>3</sub> are in good agreement with the experimental data obtained at 300 K ( $a = 3.9965 \text{ \AA}$ ,  $b = 5.8360 \text{ \AA}$ , and  $c = 5.8698 \text{ \AA}$  [6]).

In RbTaO<sub>3</sub>, the frequency of unstable  $\Gamma_{15}$  phonon in the phonon spectrum (Fig. 2) and the energy gain resulting from the transition to ferroelectric phases (Table 4) are rather low; so it is necessary to addition-

ally test the stability of the ferroelectric distortion with respect to zero-point lattice vibrations. For this purpose, we used the technique proposed in [20]. The energy gain resulting from the transition from the  $Pm3m$  phase to the  $R3m$  phase is  $E_0 = 1.90$  meV and the unstable phonon frequency at the  $\Gamma$  point in the  $Pm3m$  phase is  $\nu = 84$   $\text{cm}^{-1}$ . As the energy ratio  $h\nu/E_0 \approx 5.51$  exceeds the critical value of 2.419 obtained in [20], the energy of the lowest vibrational state in a two-well potential appears above the upper point of the energy barrier separating the potential wells, and the ferroelectric ordering is suppressed by zero-point vibrations. Therefore, the only stable phase of  $\text{RbTaO}_3$  with the perovskite structure is the cubic phase. The calculated lattice parameter of this phase is given in Table 2; its value is in satisfactory agreement with the experimental data ( $a = 4.035$   $\text{\AA}$  [6]).

It is known that the formation of phases with hexagonal  $\text{BaNiO}_3$  (polytype  $2H$ ), hexagonal  $\text{BaMnO}_3$  (polytype  $4H$ ), hexagonal  $\text{BaTiO}_3$  (polytype  $6H$ ), and rhombohedral  $\text{BaRuO}_3$  (polytype  $9R$ ) structures is characteristic of  $ABO_3$  perovskites with the tolerance factor  $t > 1$ , and the studied compounds belong to this class. Our calculations showed that the energies of these phases for both rubidium compounds are appreciably higher than the cubic phase energy (Tables 3 and 4). These results explain why it was impossible to observe the transition of  $\text{RbNbO}_3$  to the hexagonal structure [6] upon heating, by analogy to that occurring in  $\text{BaTiO}_3$ . The high energies of these phases, in particular, the  $2H$  phase, are probably caused by larger sizes and strong electrostatic repulsion of  $\text{Nb}^{5+}$  ions which occupy face-sharing octahedra in these structures.

We consider now some properties of ferroelectric  $\text{RbNbO}_3$ . The calculated polarization in  $\text{RbNbO}_3$  is  $0.46$   $\text{C/m}^2$  in the  $P4mm$  phase and  $0.50$   $\text{C/m}^2$  in the

**Table 2.** Calculated lattice parameters and atomic coordinates in  $\text{RbTaO}_3$  structures

Atom	Position	$x$	$y$	$z$
Phase $C2/m$ $a = b = 6.3396$ $\text{\AA}$ , $c = 8.0171$ $\text{\AA}$ , $\alpha = 86.1031^\circ$ , $\beta = 93.8969^\circ$ , $\gamma = 96.8997^\circ$				
Rb1	4i	+0.16000	-0.16000	+0.73758
Rb2	4g	+0.26494	+0.26494	+0.00000
Ta1	4h	+0.31104	+0.31104	+0.50000
Ta2	4i	+0.23924	-0.23924	+0.30214
O3	8j	+0.27303	+0.04639	+0.39643
O1	8j	+0.54749	-0.21209	+0.28704
O2	4i	+0.16752	-0.16752	+0.08653
O4	4i	+0.37705	-0.37705	+0.55235
Phase $Pm3m$ $a = 3.9846$ $\text{\AA}$				
Rb	1a	+0.00000	+0.00000	+0.00000
Ta	1b	+0.50000	+0.50000	+0.50000
O	3c	+0.00000	+0.50000	+0.50000

$Amm2$  and  $R3m$  phases; these values slightly exceed the calculated polarization in the same phases of  $\text{KNbO}_3$  (0.37, 0.42, and 0.42  $\text{C/m}^2$ , respectively). The static dielectric tensor in the  $R3m$  phase is characterized by two eigenvalues:  $\epsilon_{\parallel}^0 = 21.1$  and  $\epsilon_{\perp}^0 = 35.8$ ; the optical dielectric tensor eigenvalues are  $\epsilon_{\parallel}^{\infty} = 5.31$  and  $\epsilon_{\perp}^{\infty} = 5.91$ . In the cubic phase, the elastic moduli are  $C_{11} = 412$  GPa,  $C_{12} = 84$  GPa, and  $C_{44} = 102$  GPa; the bulk modulus is  $B = 193.5$  GPa. The nonzero compo-

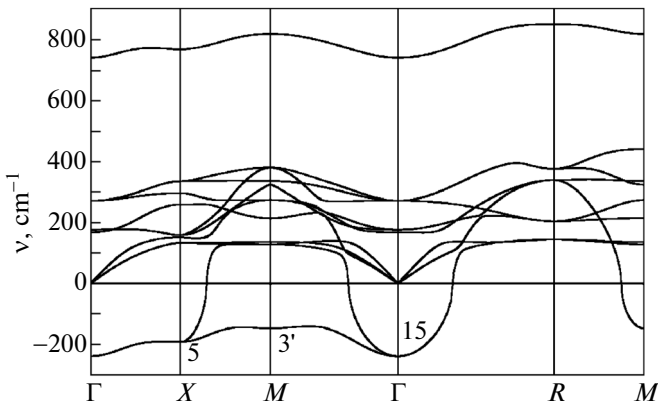


**Fig. 1.** Phonon spectrum of  $\text{RbNbO}_3$  in the cubic  $Pm3m$  phase. Labels near curves indicate the symmetry of unstable modes.

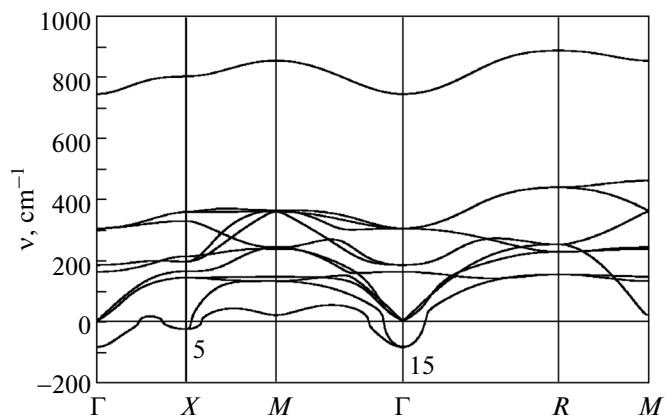


**Fig. 2.** Phonon spectrum of  $\text{RbTaO}_3$  in the cubic  $Pm3m$  phase. Labels near curves indicate the symmetry of unstable modes.

**Table 3.** Relative energies of low-symmetry RbNbO<sub>3</sub> phases formed from the cubic perovskite phase upon condensation of unstable phonons, phases with *6H*, *4H*, *9R*, and *2H* structures, and the *P* $\bar{1}$  phase prepared at atmospheric pressure (the most stable phase energy is in boldface)

Phase	Unstable mode	Energy, meV
<i>Pm</i> 3 <i>m</i>	—	0
<i>P4/nmm</i>	<i>M</i> <sub>3</sub> '	−31.3
<i>Pmma</i>	<i>X</i> <sub>5</sub>	−34.8
<i>Cmcm</i>	<i>X</i> <sub>5</sub>	−38.7
<i>P4mm</i>	$\Gamma_{15}$	−46.5
<i>Amm</i> 2	$\Gamma_{15}$	−57.0
<i>R3m</i>	$\Gamma_{15}$	<b>−58.6</b>
<i>P</i> $\bar{1}$	—	+27.4
<i>P6</i> <sub>3</sub> / <i>mmc</i> ( <i>6H</i> )	—	+121.4
<i>P6</i> <sub>3</sub> / <i>mmc</i> ( <i>4H</i> )	—	+334.0
<i>R</i> $\bar{3}m$ ( <i>9R</i> )	—	+568.1
<i>P6</i> <sub>3</sub> / <i>mmc</i> ( <i>2H</i> )	—	+1752

nents of the tensors of piezoelectric effect  $e_{iv}$ , second-order nonlinear optical susceptibility  $d_{iv}$ , and linear electro-optic (Pockels) effect  $r_{iv}$  in the *R3m* phase of rubidium niobate are compared with the corresponding properties of other rhombohedral ferroelectrics in Table 5. We can see that the piezoelectric moduli in rhombohedral RbNbO<sub>3</sub> (as well as in its other polar phases) are slightly lower than in KNbO<sub>3</sub>. The nonlinear optical coefficients in RbNbO<sub>3</sub> exceed the corresponding values in KNbO<sub>3</sub>, although the  $d_{33}$  value in rubidium niobate is slightly lower than in lithium niobate. As for the electro-optical properties, in rhombohedral RbNbO<sub>3</sub> they are slightly lower than in KNbO<sub>3</sub>, but are notably superior to those of lithium niobate. In the orthorhombic phase (stable at 300 K), nonlinear optical properties of RbNbO<sub>3</sub> are comparable to those of the same phase of potassium niobate: for example, the  $d_{33}$  modulus is −30.8 pm/V in RbNbO<sub>3</sub> and −30.4 pm/V in KNbO<sub>3</sub>.

In cubic RbTaO<sub>3</sub>, the optical dielectric constant is  $\epsilon_{\infty} = 5.58$ . The static dielectric constant can be estimated only in the rhombohedral phase as  $\sim 140$ . The elastic moduli in cubic rubidium tantalate are  $C_{11} = 466$  GPa,  $C_{12} = 91.5$  GPa, and  $C_{44} = 120$  GPa;  $B = 216$  GPa. The piezoelectric moduli, second-order nonlinear optical susceptibility, and electro-optical coefficients in the cubic phase are zero.

An unexpected result of our calculations is that in both studied compounds the *P* $\bar{1}$  and *C2/m* phases which can be prepared at atmospheric pressure are metastable. This result is probably caused by an effec-

**Table 4.** Relative energies of low-symmetry RbTaO<sub>3</sub> phases formed from the cubic perovskite phase upon condensation of unstable phonons, phases with *6H*, *4H*, *9R*, and *2H* structures, and the *C2/m* phase prepared at atmospheric pressure (the most stable phase energy is in boldface)

Phase	Unstable mode	Energy, meV
<i>Pm</i> 3 <i>m</i>	—	0
<i>P4mm</i>	$\Gamma_{15}$	−1.80
<i>Amm</i> 2	$\Gamma_{15}$	−1.87
<i>R3m</i>	$\Gamma_{15}$	<b>−1.90</b>
<i>C2/m</i>	—	+38.5
<i>P6</i> <sub>3</sub> / <i>mmc</i> ( <i>6H</i> )	—	+113.3
<i>P6</i> <sub>3</sub> / <i>mmc</i> ( <i>4H</i> )	—	+352.2
<i>R</i> $\bar{3}m$ ( <i>9R</i> )	—	+589.0
<i>P6</i> <sub>3</sub> / <i>mmc</i> ( <i>2H</i> )	—	+1839

tive lattice contraction which always exists in the LDA calculations. The fact that the specific volume of the *Pm*3*m* phase is noticeably smaller than that of *P* $\bar{1}$ , *C2/m*, *P6*<sub>3</sub>/*mmc*, and *R* $\bar{3}m$  phases suggests that under pressure the cubic perovskite phase will be the most stable one. To estimate the maximum value of the actual effective pressure, the lattice parameters and atomic positions in the *C2/m* structure of rubidium tantalate were calculated for different pressures and it was shown that the unit cell volume equal to the experimental one at 300 K can be obtained at an isotropic pressure of −24.7 kbar. At this pressure, the enthalpy of the *C2/m* phase becomes lower than that of *Pm*3*m* by  $\sim 230$  meV, i.e., becomes consistent with the experimental data. At the above mentioned negative pressure, the ratio  $h\nu/E_0$  determining the stability of the ferroelectric phase in RbTaO<sub>3</sub> becomes equal to 1.90, i.e., slightly less than the critical value of 2.419. However, if we take into account that the above negative pressure is obviously overestimated, since it includes the thermal expansion effect, we can suppose that, even taking into account the systematic error in the LDA lattice parameter determination, rubidium tantalate will remain cubic up to the lowest temperatures.

The conclusion that RbTaO<sub>3</sub> is an incipient ferroelectric in which the ferroelectric ordering is suppressed by zero-point vibrations agrees with the data of [6], but contradicts the data of [1] in which the phase transition near 520 K was reported. We suppose that tantalum-enriched phases (in particular, with the tungsten-bronze structure [8]) could be formed in rubidium tantalate samples discussed in [1] because of the low temperature of the peritectic reaction, and this could result in the observed anomaly.

In [11], the possibility of using various oxides with the perovskite structure, in particular RbNbO<sub>3</sub> and

**Table 5.** Nonzero components of the piezoelectric tensor  $e_{iv}$  (C/m<sup>2</sup>) and tensors of the second-order nonlinear optical susceptibility  $d_{iv}$  and the linear electro-optic effect  $r_{iv}$  (pm/V) in rhombohedral phases of RbNbO<sub>3</sub>, KNbO<sub>3</sub>, LiNbO<sub>3</sub>, and BaTiO<sub>3</sub>

Coefficient	RbNbO <sub>3</sub>	KNbO <sub>3</sub>	LiNbO <sub>3</sub>	BaTiO <sub>3</sub>
$e_{11}$	-3.0	-4.2	-2.4	-4.0
$e_{15}$	+4.8	+6.8	+3.5	+7.3
$e_{31}$	+2.4	+2.3	+0.1	+3.5
$e_{33}$	+2.9	+3.1	+1.1	+5.1
$d_{11}$	+12.7	+11.9	+2.3	+4.4
$d_{15}$	-23.6	-21.9	-11.5	-16.1
$d_{31}$	-23.6	-21.9	-11.5	-16.1
$d_{33}$	-29.4	-27.3	-37.4	-31.1
$r_{11}$	-12.8	-17.7	-5.6	-13.7
$r_{15}$	+27.6	+39.2	+17.1	+43.3
$r_{31}$	+18.0	+23.9	+10.1	+25.3
$r_{33}$	+30.1	+40.6	+27.3	+48.9

RbTaO<sub>3</sub>, for development of photoelectrochemical solar cells was discussed. We calculated the band gap  $E_g$  in these compounds both in the LDA approximation and in the  $GW$  approximation that takes into account many-body effects (the technique of the latter calculations was analogous to that used in [21–23]). In the LDA approximation,  $E_g^{\text{LDA}} = 1.275$  eV in cubic RbNbO<sub>3</sub> when the spin–orbit coupling is neglected; in  $P4mm$ ,  $Amm2$ , and  $R3m$  phases,  $E_g^{\text{LDA}}$  is 1.314, 1.869, and 2.137 eV, respectively. In cubic RbTaO<sub>3</sub>,  $E_g^{\text{LDA}} = 2.175$  eV when the spin–orbit coupling is neglected. The valence band extrema in the cubic phase of both compounds are at the  $R$  point of the Brillouin zone, whereas the conduction band extrema are at the  $\Gamma$  point. The calculations using the technique of [23] yield the spin–orbit splitting of the conduction band edge  $\Delta_{SO} = 0.111$  eV for RbNbO<sub>3</sub> and  $\Delta_{SO} = 0.400$  eV for RbTaO<sub>3</sub>; the spin-orbit splitting of the valence band edge is absent. After correction for the conduction band edge shift ( $\Delta_{SO}/3$ ), the LDA values of  $E_g$  that take into account the spin–orbit coupling are 1.238, 1.277, 1.832, 2.100, and 2.042 eV for four RbNbO<sub>3</sub> phases and for cubic RbTaO<sub>3</sub>, respectively.

In the  $GW$  approximation, the band gap when the spin–orbit coupling is neglected is  $E_g^{\text{GW}} = 2.403$ , 2.616, 3.291, and 3.609 eV, respectively in cubic, tetragonal, orthorhombic, and rhombohedral RbNbO<sub>3</sub> and 3.302 eV in cubic RbTaO<sub>3</sub>. If the spin–orbit coupling is taken into account, these values decrease to 2.366, 2.579, 3.254, 3.572, and 3.169 eV, respectively.

The obtained values of  $E_g$  are appreciably smaller than those calculated in [11] for cubic phases (3.4 eV for RbNbO<sub>3</sub> and 4.3 eV for RbTaO<sub>3</sub>).

Some authors who studied rubidium niobate and rubidium tantalate have noticed their sensitivity to humidity. Evidently, this can be a serious obstacle for practical applications of these materials. However, we would like to note that this property is inherent to phases prepared at atmospheric pressure and having “loose” structures whose specific volume is 26–28% larger than that of the perovskite phase. In [8], it was suggested that the effect is due to intercalation of water molecules into the “loose” structures, rather than to hydrolysis of these compounds. The possibility of preparing RbTaO<sub>3</sub> by hydrothermal synthesis [24] and the low rate of RbTaO<sub>3</sub> ion exchange in HCl during its delamination [12] support this idea. This suggests that the considered compounds with the perovskite structure can be quite stable to humidity.

Thus, the present calculations of RbNbO<sub>3</sub> and RbTaO<sub>3</sub> properties and their comparison with the properties of other ferroelectrics show that rubidium niobate is an interesting ferroelectric material with high nonlinear optical and electro-optical properties, and rubidium tantalate is an incipient ferroelectric.

The calculations presented in this work were performed on the laboratory computer cluster (16 cores).

#### ACKNOWLEDGMENTS

This work was supported by the Russian Foundation for Basic Research (project no. 13-02-00724).

#### REFERENCES

1. G. A. Smolenskii and N. V. Kozhevnikova, Dokl. Akad. Nauk SSSR **76**, 519 (1951).
2. H. D. Megaw, Acta Crystallogr. **5**, 739 (1952).
3. M. Serafin and R. Hoppe, J. Less-Common Met. **76**, 299 (1980).
4. M. Serafin and R. Hoppe, Angew. Chem. **90**, 387 (1978).
5. M. Serafin and R. Hoppe, Z. Anorg. Allg. Chem. **464**, 240 (1980).
6. J. A. Kafalas, in *Proceedings of the 5th Materials Research Symposium, Gaithersburg, Maryland, United States, October 18–21, 1971* (NBS Spec. Publ., No. 364, 287 (1972)).
7. A. Reisman and F. Holtzberg, J. Phys. Chem. **64**, 748 (1960).
8. H. Brusset, H. Gillier-Pandraud, M. Chubb, and R. Mahé, Mater. Res. Bull. **11**, 299 (1976).
9. D. F. O’Kane, G. Burns, E. A. Giess, B. A. Scott, A. W. Smith, and B. Olson, J. Electrochem. Soc. **116**, 1555 (1969).
10. G. Burns, E. A. Giess, and D. F. O’Kane, US Patent No. 3 640 865 (1972).

11. I. E. Castelli, D. D. Landis, K. S. Thygesen, S. Dahl, I. Chorkendorff, T. F. Jaramillo, and K. W. Jacobsen, *Energy Environ. Sci.* **5**, 9034 (2012).
12. K. Fukuda, I. Nakai, Y. Ebina, R. Ma, and T. Sasaki, *Inorg. Chem.* **46**, 4787 (2007).
13. *The ABINIT code is a common project of the Université Catholique de Louvain, Corning Incorporated and other contributions.* <http://www.abinit.org/>.
14. A. I. Lebedev, *Phys. Solid State* **52** (7), 1448 (2010).
15. A. M. Rappe, K. M. Rabe, E. Kaxiras, and J. D. Joannopoulos, *Phys. Rev. B: Condens. Matter* **41**, 1227 (1990).
16. *Opium—Pseudopotential Generation Project.* <http://opium.sourceforge.net/>.
17. A. I. Lebedev, *Phys. Solid State* **51** (2), 362 (2009).
18. M. Veithen, X. Gonze, and P. Ghosez, *Phys. Rev. B: Condens. Matter* **71**, 125107 (2005).
19. R. Yu and H. Krakauer. *Phys. Rev. Lett.* **74**, 4067 (1995).
20. A. I. Lebedev, *Phys. Solid State* **51** (4), 802 (2009).
21. A. I. Lebedev, *Phys. Solid State* **54** (8), 1663 (2012).
22. A. I. Lebedev, *J. Alloys Compd.* **580**, 487 (2013).
23. A. I. Lebedev, *Phys. Solid State* **56** (5), 1039 (2014).
24. D. Gompel, M. N. Tahir, M. Panthofer, E. Mugnaioli, R. Brandscheid, U. Kolb, and W. Tremel, *J. Mater. Chem. A* **2**, 8033 (2014).

*Translated by A. Kazantsev*